

Electron mobilities in dimensional subbands of combinatively doped GaAs/GaAlAs heterojunctions with high density of 2D electrons

V. A. Kul'bachinskiĭ, R. A. Lunin, V. G. Kytin, A. S. Bugaev, and A. P. Senichkin

M. V. Lomonosov Moscow State University, 119899 Moscow, Russia

(Submitted 17 April 1996)

Zh. Ėksp. Teor. Fiz. **110**, 1517–1532 (October 1996)

The paper reports about a study of the Shubnikov–de Haas effect, quantum Hall effect, and electric transport parameters of GaAs/Al_xGa_{1-x}As heterostructures in which the Al_xGa_{1-x}As is uniformly doped with silicon and GaAs is δ -doped at various distances L_δ between the δ -layer and heterojunction. Measurements have been performed at temperatures ranging between 0.4 K and 300 K in magnetic fields of up to 35 T. The conductivity and Hall mobility were measured as functions of L_δ . The maximum Hall mobility and 2D-electron conductivity were observed at $L_\delta=600\text{--}750$ Å. The sheet density, transport and quantum mobilities of 2D-electrons in different dimensional subbands have been evaluated from the transverse magnetoresistance. The transport mobility in the highest subband is an order of magnitude higher than in the lowest subband owing to the separation between free electrons and ionized impurities. The self-consistent solution of the Schrödinger and Poisson equations yields the electron densities, effective masses, and wave functions in all subbands. The electron mobility due to scattering from ionized impurities has been calculated when several subbands are occupied. The differences among transport and quantum mobilities in the subbands of GaAs/AlGaAs heterostructures with combined doping at low temperatures have been interpreted in terms of scattering from ionized impurities. © 1996 American Institute of Physics. [S1063-7761(96)02710-2]

1. INTRODUCTION

Two-dimensional semiconductor structures with high electron densities where two or more dimensional subbands are filled generate a lot of interest.¹⁻⁸ The behavior of electrons in such systems is more complicated than in structures where only one subband is filled. An essential factor is intersubband electron scattering;⁵⁻⁹ the electron mobilities in the subbands are different. High densities of two-dimensional (2D) electrons can be generated by δ -doping, which has been studied fairly intensively.¹⁰⁻¹⁴ Besides, the task of fabricating high-power field-effect transistors based on heterostructures demands higher 2D electron densities.

This paper reports a study of GaAs/Al_xGa_{1-x}As heterojunctions in which not only is the AlGaAs layer uniformly doped with silicon, but the GaAs layer is δ -doped. Using this combined doping, we could fabricate heterostructures with higher 2D-electron densities and a sufficiently high Hall mobility of current carriers.

The main task of our work was to measure the quantum oscillations of magnetoresistance and the quantum Hall effect in high magnetic fields (up to 35 T) and low temperatures (down to 0.4 K) in manufactured structures where many subbands of dimensional quantization are filled with electrons with a view to determine transport and quantum mobilities of 2D electrons in the subbands as functions of the separation L_δ between the δ -layer and heterojunction. We have calculated the electronic band structure and wave functions at various L_δ , and the transport and quantum mobilities of electrons in all the subbands with due account of the intersubband scattering from ionized impurities.

2. EXPERIMENTAL TECHNIQUES AND SAMPLES

Techniques of measuring resistance and magnetoresistance as functions of temperature

The resistance versus temperature was measured in the range of 0.4 to 300 K, and the Hall effect and transverse magnetoresistance were measured in the range of 0.4 to 150 K in a dc magnetic field of up to 12 T and in a pulsed magnetic field of up to 35 T.

The temperature was lowered to 0.4 K by pumping out vapor of liquid ³He. In the range of 4.2–300 K, the temperature was measured using a copper–iron thermocouple, and in the range of 0.4–4.2 K using a carbon resistance thermometer.

The conductivity and Hall effect were measured in the double Hall bridge configuration by the dc method using a low-frequency current bridge.

In measurements of the magnetoresistance or Hall effect at low temperatures in a magnetic field of up to 12 T, we used a superconducting solenoid, while the measurements in a magnetic field of up to 35 T were performed at the pulsed magnetic facility of Amsterdam University.

Structure of the samples

We used GaAs/AlGaAs heterostructures with combined doping grown by molecular-beam epitaxy. A diagram of the sample structure is given in Fig. 1. A 1- μ m buffer layer of *i*-GaAs was grown at 550 °C on a semi-insulating GaAs(Cr) substrate, then a silicon δ -layer with a density of $N_s=1.5\times 10^{13}$ cm⁻² was deposited on the surface and coated with an *i*-GaAs layer with a thickness L_δ . Next a

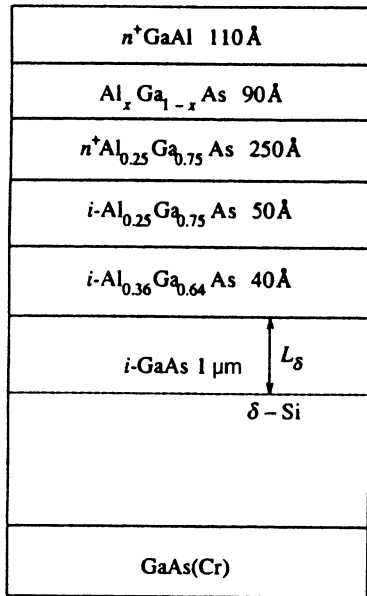


FIG. 1. Diagram of the structure of investigated samples.

conventional heterojunction was manufactured by growing an $i\text{-Al}_x\text{Ga}_{1-x}\text{As}$ spacer with a thickness of 40 Å ($x=0.36$) or 50 Å ($x=0.25$), a doped layer of $n\text{-Al}_{0.25}\text{Ga}_{0.75}\text{As}$ 250 Å thick, and an $i\text{-Al}_x\text{Ga}_{1-x}\text{As}$ layer with a variable gap width 90 Å thick (the parameter x varied from 0.25 to 0). This barrier was manufactured in order to block formation of DX-centers and of a parallel conducting channel. The structure was capped with a GaAs contact layer 110 Å thick. The silicon δ -layer was located in the samples with numbers running from 1 to 6 at distances $L_\delta=200, 400, 600, 750, 1000,$ and 1200 Å from the heterojunction. The measured structures were defined in the shape of a double Hall bridge with a channel width of $150 \mu\text{m}$ by the photolithographic technique.

3. PARAMETERS OF 2D ELECTRON GAS IN THE INVESTIGATED HETEROSTRUCTURES

Conductivity and magnetoresistance of GaAs/GaAlAs heterostructures with combined doping

The resistances of all the samples drop as the temperature rises up to 50–100 K, then the resistance changes with

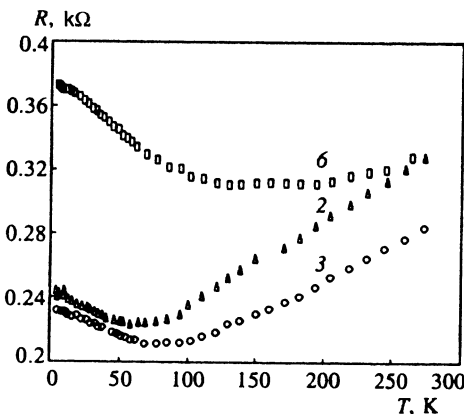


FIG. 2. Sheet resistances of samples 2, 3, and 6 versus temperature.

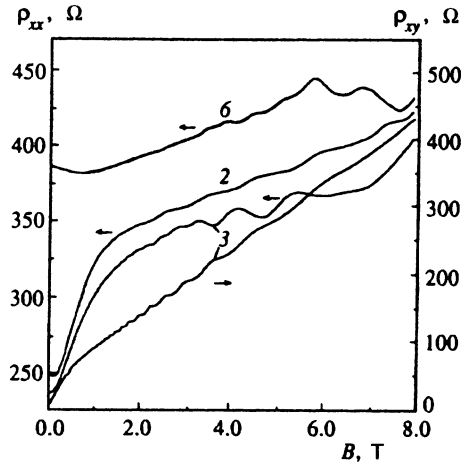


FIG. 3. Transverse magnetoresistance ρ_{xx} (samples 2, 3, and 6) and Hall magnetoresistance ρ_{xy} (sample 3) at $T=0.4$ K.

temperature like that of metals. Figure 2 shows as an example the sheet resistances of samples 2, 3, and 6 versus temperature.

Shubnikov–de Haas oscillations were detected in the heterostructures in strong magnetic fields and at low temperatures. The resistivity components ρ_{xx} for the samples 2, 3, and 6, and ρ_{xy} for the sample 3 versus magnetic field ranging up to 8 T at a temperature of 0.4 K are shown in Fig. 3. The transverse resistivity ρ_{xx} and Hall resistivity ρ_{xy} of samples 3 and 6 versus magnetic field ranging to 35 T at a temperature of 4.2 K are given in Fig. 4. Analysis of the magnetoresistance oscillations yields fairly accurate determination of the 2D electron density and mobility in the dimensional quantization subbands, which will be discussed below.

Hall effect measurements indicate that in all the samples the Hall coefficient R is constant with temperature in the range of 0.4 to 10 K. Therefore the curves of $\rho(T)$ shown in Fig. 2 demonstrate the temperature dependence of the

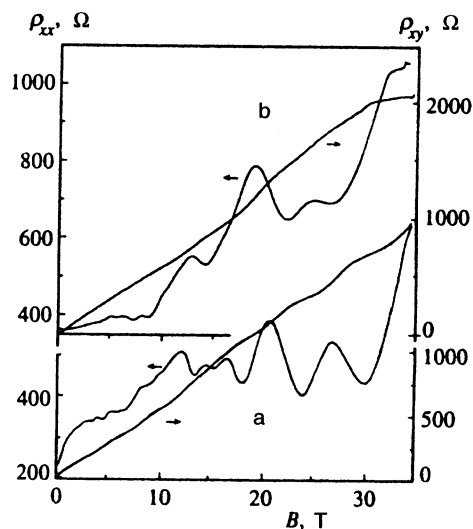


FIG. 4. Shubnikov–de Haas oscillations of ρ_{xx} and Hall resistivity ρ_{xy} (a) samples 3 and (b) 6 at $T=4.2$ K.

electron mobility. The sheet conductance of the samples $\sigma \approx (3-4.5) \times 10^{-3} \Omega^{-1}$ at the liquid-helium temperature is higher than in previously studied δ -doped heterostructures: $\sigma \approx (1-1.5) \times 10^{-3} \Omega^{-1}$,⁷ $\sigma \approx (1-2.5) \times 10^{-3} \Omega^{-1}$,¹⁵ $\sigma \approx (2-3) \times 10^{-3} \Omega^{-1}$,¹⁶ $\sigma \approx 3 \times 10^{-3} \Omega^{-1}$,¹⁷ $\sigma \approx (2.5-3.5) \times 10^{-3} \Omega^{-1}$.¹⁸

Determination of electron densities and mobilities using the Shubnikov–de Haas effect

Reliable electron densities can be derived from Shubnikov–de Haas oscillations, for which each subband has an oscillation with its own period. The part of the density of states oscillating in the magnetic field, Δg , can be expressed as^{19–21}

$$\frac{\Delta g(E_F)}{g_0} = 2 \sum_{s=1}^{\infty} \exp\left(-\frac{\pi s}{\mu_q B}\right) \cos\left[\frac{2\pi s E_F}{\hbar \omega_c} - s\pi\right] \frac{sX}{\sinh(sX)},$$

$$X = \frac{2\pi^2 kT}{\hbar \omega_c}, \quad (1)$$

which leads to the following expressions for the conductivity tensor components in the two-dimensional case (the Landau level width Γ is assumed to be independent of energy and magnetic field, and $\tau_q = \hbar/2\Gamma$):

$$\sigma_{xx} = \frac{eN_s \mu_0}{1 + \mu_0^2 B^2} \left[1 + \frac{2\mu_0^2 B^2 \Delta g(E_F)}{(1 + \mu_0^2 B^2)g_0} \right], \quad (2)$$

$$\sigma_{xy} = -\frac{eN_s \mu_0^2 B}{1 + \mu_0^2 B^2} \left[1 - \frac{3\mu_0^2 B^2 + 1}{\mu_0^2 B^2 (1 + \mu_0^2 B^2)} \frac{\Delta g(E_F)}{g_0} \right], \quad (3)$$

where $\mu_0 = e\tau_0/m^*$ is the transport mobility at $B=0$, g_0 is the density of states at zero magnetic field, $\mu_q = e\tau_q/m^*$ is the ‘‘quantum’’ mobility, N_s is the electron density, and e is the absolute value of the electron charge. The oscillation frequency B_p in the reciprocal magnetic field determines the two-dimensional electron density: $N_s = eB_p/\pi\hbar$, $E_F = (\pi\hbar^2/m^*)N_s$. If several subbands are filled, the conductivities due to their carriers should be added.

In order to separate the oscillating component, the resistance should be differentiated twice with respect to the reciprocal magnetic field $u = 1/B$. An application of this technique to the determination of electron density in subbands is illustrated by Fig. 5, which shows curves for sample 3. The resistivity ρ_{xx} versus the reciprocal magnetic field u (Fig. 5a) has been numerically differentiated (Fig. 5b), and a fast Fourier transform has been performed (Fig. 5c).

Analysis of the oscillation amplitude as a function of magnetic field and temperature yields the mobility of 2D electrons in each dimensional subband. But here we face the problem related to the difference between the transport and quantum mobilities, μ_0 and μ_q .^{8,9,22–24} The transport relaxation time τ_0 of the electron momentum is derived by solving the Boltzmann kinetic equation in the relaxation-time approximation and can be expressed as^{17,25}

$$\frac{1}{\tau_0} = \int_0^\pi Q(\theta)(1 - \cos \theta) d\theta, \quad (4)$$

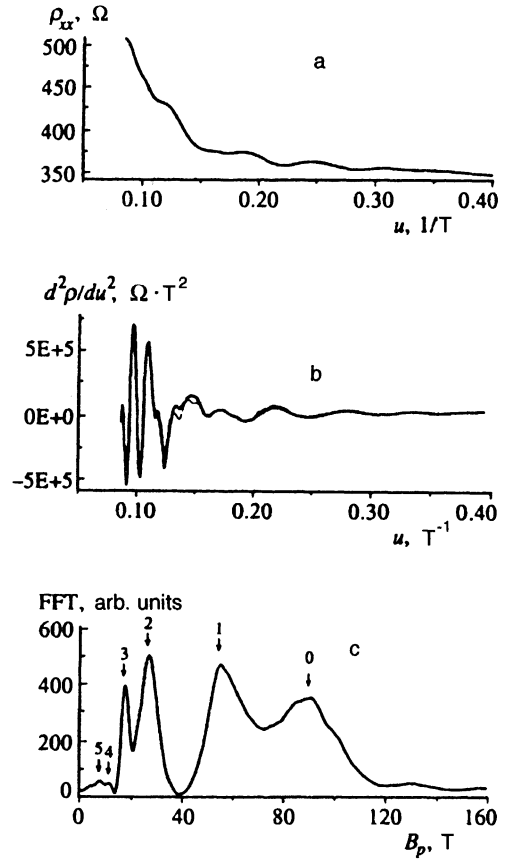


FIG. 5. Determination of electron densities and mobilities: (a) experimental curve of magnetoresistance versus reciprocal magnetic field $u = 1/B$; (b) second derivative of the oscillating function $\partial^2 \rho_{xx}(u)/\partial u^2$ (thin line shows calculations with parameters listed in Table I); (c) Fourier transform of $\partial^2 \rho_{xx}(u)/\partial u^2$. Measurements were taken from sample 3 at a temperature of 4.2 K.

where $Q(\theta)$ is proportional to the probability of scattering through the angle θ , while the quantum relaxation time is defined by the equation^{21,26}

$$\frac{1}{\tau_q} = \int_0^\pi Q(\theta) d\theta. \quad (5)$$

Because of the factor $1 - \cos \theta$ in the equation for τ_0 , scattering through small angles makes a negligible contribution, and if $Q(\theta)$ is largest at small angles (for example, in the case of Coulomb scattering), the transport relaxation time τ_0 may be an order of magnitude larger than τ_q .

By varying μ_0 and μ_q in each subband, one can fit the second derivative of $\rho_{xx} = \sigma_{xx}/(\sigma_{xx}^2 + \sigma_{xy}^2)$ with respect to u calculated using Eqs. (1)–(3) to experimental data. The fit to measurements of the sample 3 is shown in Fig. 5b by the light trace. In this fit we used the optimization technique described in Ref. 27. The resulting parameters N_s , μ_0 , and μ_q are listed in Table I. By and large, there is a tendency to higher mobilities (both transport and quantum) as the subband number increases. The transport mobility is a factor of two to three larger than the quantum mobility. The following ratios of the transport to quantum mobility were obtained by different researchers of heterostructures based on GaAs: $\mu_0/\mu_q \approx 2.5$ (Ref. 17), $\mu_0/\mu_q \approx 4-9$ (Ref. 21), μ_0/μ_q

TABLE I. 2D densities N_s and effective masses m^* of electrons in dimensional subbands derived from self-consistent calculations; electron densities, transport μ_0 and quantum μ_q mobilities derived from Shubnikov–de Haas measurements at a temperature of 4.2 K; transport μ_0 and quantum μ_q mobilities calculated for scattering from ionized impurities, including intersubband scattering for the samples 2, 3, and 6.

Sample number	n Subband number	Self-consistent calculation		Shubnikov–de Haas			Calculation	
		N_s , 10^{12} cm^{-2}	m^*/m_0	N_s , 10^{12} cm^{-2}	μ_0 , $\text{cm}^2/\text{V}\cdot\text{s}$	μ_q , $\text{cm}^2/\text{V}\cdot\text{s}$	μ_0 , $\text{cm}^2/\text{V}\cdot\text{s}$	μ_q , $\text{cm}^2/\text{V}\cdot\text{s}$
2	0	4.32	0.069	4.27	1400	700	1860	700
	1	2.94	0.072	2.83	1680	790	2000	740
	2	1.62	0.073	1.75	1800	900	2600	1010
	3	0.74	0.073	0.93	3500	2200	3700	2140
	4	0.52	0.068	0.48	-	-	12000	8600
	5	0.25	0.070	-	-	-	5300	3600
3	0	4.59	0.069	4.68	1560	530	1670	700
	1	2.78	0.072	2.66	1700	800	1950	740
	2	1.44	0.073	1.51	2480	900	2350	1020
	3	0.79	0.072	0.75	3300	2300	2970	1630
	4	0.48	0.068	0.45	-	-	$>10^5$	$>10^5$
	5	0.27	0.070	0.36	-	-	4480	3160
6	0	4.36	0.069	4.46	1410	480	1610	760
	1	2.40	0.073	2.00	1530	670	2100	1180
	2	1.32	0.072	1.60	2300	790	3000	2300
	3	0.48	0.068	0.49	-	-	$>10^5$	$>10^5$
	4	0.46	0.070	-	-	-	4530	3860
	5	0.14	0.069	-	-	-	9400	9010

$\approx 5-9$ (Ref. 9), $\mu_0/\mu_q \approx 4-16$ (Ref. 25). These values of the mobilities may be inaccurate because the quantum limit is achieved in the fifth subband at a magnetic field of 6–8 T.

Table I also lists electron densities and effective masses derived from a self-consistent solution of the Poisson and Schrödinger equations, and electron mobilities calculated by taking account of the electron scattering from ionized impurities, including intersubband scattering. The calculation techniques and results will be discussed below.

The transport mobility and electron density in the samples can be also derived from measurements of the classical magnetoresistance.^{28,29} In this technique the measurements of ρ_{xx} and ρ_{xy} as functions of magnetic field are transformed to the so-called mobility spectrum, which yields the peak conductivity as a function of mobility. The parameters ρ_{xx} and ρ_{xy} for the samples 2, 3, and 6 measured in the magnetic field range of 0.2 to 1.5 T were transformed to the mobility spectrum, which demonstrated that the samples contained two groups of electrons with lower ($\approx 1800 \text{ cm}^2/\text{V}\cdot\text{s}$) and higher ($\approx 20000 \text{ cm}^2/\text{V}\cdot\text{s}$) mobilities.

At low magnetic field of less than 0.02 T for the samples 2 and 3 and less than 0.2 T for the sample 6, a small negative magnetoresistance was detected, whereas the Shubnikov–de Haas oscillations were observed only in magnetic fields beyond 2 T (Fig. 3). The absolute value of the negative magnetoresistance drops with the temperature. Along with the increase in the sample resistance at low temperatures ($T < 40 \text{ K}$) at a constant electron density (Fig. 2), this negative magnetoresistance may be ascribed to quantum corrections to conductivity in two-dimensional structures.³⁰

4. CALCULATION OF ELECTRON BANDS AND TRANSPORT PARAMETERS OF HETEROSTRUCTURES

Scheme of the self-consistent calculation of electronic bands in heterojunctions

The electron wave functions $\psi_n(z)$ and energies E_n are determined in the effective mass approximation by the one-dimensional Schrödinger equation

$$\left[-\frac{\hbar^2}{2} \frac{d}{dz} \left(\frac{1}{m^*(z)} \frac{d}{dz} \right) + U(z) \right] \psi_n(z) = E_n \psi_n(z). \quad (6)$$

The potential energy $U(z) = U_c(z) + U_H(z) + U_{xc}(z)$ is the sum of the jump in the conduction band energy U_c on the heterojunction, electrostatic potential energy U_H (Hartree potential), and exchange-correlation potential U_{xc} . The electron effective mass in $\text{Al}_x\text{Ga}_{1-x}\text{As}$ is described by the formula²³ $m^*(z) = (0.0665 + 0.0835x)m_0$, where m_0 is the free-electron mass. The difference between the gap widths in GaAs and $\text{Al}_x\text{Ga}_{1-x}\text{As}$ equals³¹ $\Delta E_g = (1155x + 370x^2) \text{ meV}$. The ratio of the potential jump at the conduction band bottom to that of the gap width was taken to be $\Delta E_c/\Delta E_g \approx 0.63$ (Refs. 32 and 33), implying $U_c(z) = 0.63(1155x + 370x^2) \text{ meV}$. The electrostatic potential energy is determined by the Poisson equation

$$\frac{d}{dz} \left(\varepsilon_0 \varepsilon(z) \frac{dU_H(z)}{dz} \right) = -e^2 \left[\sum N_{s_n} \psi_n^2(z) - N_I(z) \right] \quad (7)$$

where ε_0 is the permittivity of free space, ε is the material dielectric constant, and N_I is the three-dimensional density of ionized impurities (donors and acceptors): $N_I = N_d - N_a$. The number of electrons in the n th subband is

$$N_{s_n} = \frac{m^*}{\pi \hbar^2} kT \ln \left[1 + \exp \left(\frac{E_F - E_n}{kT} \right) \right]. \quad (8)$$

Assuming that the Fermi level of the system at $T=0$ K far from the heterojunction coincides with the donor level, $U(-\infty) = E_{b1}$, $U(+\infty) = E_{b2}$ (the energy is measured with respect to the Fermi level, $E_F = 0$), and that $\psi|_{z \rightarrow \pm\infty} = 0$, we obtain the boundary conditions in the form

$$U_H|_{z \rightarrow \pm\infty} = E_b - U_c|_{z \rightarrow \pm\infty}, \quad \left. \frac{dU_H(z)}{dz} \right|_{z \rightarrow \pm\infty} = 0. \quad (9)$$

The exchange-correlation energy is, generally speaking, an unknown functional of the electron density, $U_{xc}(z) = U_{xc}[n(z)]$. In practical calculations, a simple approximation for the exchange-correlation contribution, namely the local-density approach, is commonly used. In this approximation we have $U_{xc}[n(z)] = \mu_{xc}[n_0 = n(z)]$, where μ_{xc} is the exchange-correlation contribution to the chemical potential of a uniform electron gas with constant density n_0 equal to the local electron density $n(z)$ in the inhomogeneous system. The function U_{xc} was approximated by the formula³⁴

$$U_{xc} = - \left[1 + 0.0545 r_s \ln \left(1 + \frac{11.4}{r_s} \right) \right] \frac{2}{\pi a r_s} \text{Ry}^*, \quad (10)$$

where

$$\alpha = \left(\frac{4}{9\pi} \right)^{1/3}, \quad r_s = \left(\frac{4\pi a_B^3 n(z)}{3} \right)^{-1/3},$$

$$a_B^* = \frac{4\pi \epsilon_0 \epsilon \hbar^2}{m^* e^2}, \quad \text{Ry}^* = \frac{e^2}{8\pi \epsilon_0 \epsilon a_B^*}.$$

In gallium arsenide the effective Bohr radius is $a_B^* \approx 100$ Å, and the effective Rydberg is $\text{Ry}^* \approx 5.4$ meV.

The difference between the dielectric constants of GaAs and $\text{Al}_x\text{Ga}_{1-x}\text{As}$ gives rise to an image force acting on an electron near the heterojunction. The difference between the dielectric constants of the two materials, however, is no more than 10%, so we ignored the contribution of this effect to the potential energy.³⁵

In the absence of charges, the energy $U_c(z)$ at the bottom of the conduction band has a jump on the heterojunction. In order to smooth this jump on the junction, the function $U_c(z)$ was multiplied by the interpolation function $G(z)$, whose exact form was given by Stern and Das Sarma.³⁵

The one-dimensional Schrödinger equation was solved using the transfer matrix technique.³⁶ The calculation took into account the nonparabolicity of the conduction band, which is significant at large subband energies.³⁷ The nonparabolicity leads to the following corrections: (1) the energies of subband edges are slightly lowered; (2) the effective masses in the subbands with higher numbers in the δ -layer are enhanced by up to 7% (see Table I).

Band diagrams of the heterostructures

The self-consistent solution of the Schrödinger and Poisson equations was found using an iteration algorithm which included the following steps.

1) An initial potential energy U_{in} was selected and the Schrödinger equation (6) was solved. Thus we obtained the energy levels E_n and wave functions $\psi_n(z)$ in the selected potential.

2) The corrections to the energy levels and electron effective masses due to the nonparabolicity were calculated.

3) 2D electron densities in the subbands were calculated using Eq. (8).

4) The Poisson equation (7) was solved. The density of ionized donors in the δ -layer was selected so that the total electron density in all the subbands should equal the experimental value derived from Shubnikov–de Haas oscillations.

5) The potential jump $U_c(z)$ and exchange correlation energy $E_{xc}(z)$ from Eq. (10) were added to the electrostatic potential $U_H(z)$, yielding the total potential energy $U_{out}(z)$.

6) If U_{out} were very close to U_{in} (for example, $\max|U_{out}(z) - U_{in}(z)| < 0.1$ meV), U_{out} was defined as the solution and the process was terminated; otherwise a new initial potential $U_{in}^{new} = U_{in}^{old} + k(U_{out} - U_{in}^{old})$ was introduced: and steps 1 to 6 were repeated. The coefficient k was introduced for better convergence of the iteration procedure; we took $k \approx 0.01$. The silicon level energy was taken to be $E_b = 5.8$ meV. The donor density in $\text{Al}_{0.25}\text{Ga}_{0.75}\text{As}$ was $3 \times 10^{17} \text{ cm}^{-3}$. The effect of acceptors was neglected.

In order to fit the calculated electron densities in the subbands to the experimental data, we had to assume that the δ -layer had a finite thickness. Supposing that the donors were uniformly distributed in a layer with a thickness Δz , we found the Δz at which the agreement with the experimental data was the best. This method for determination of the δ -layer thickness was used by several authors.^{38–41} Using this technique, Zrenner *et al.*¹⁶ obtained $\Delta z = 80$ Å in structures grown at $T_s = 530$ °C at a 2D electron density of $N_s = 8 \times 10^{12} \text{ cm}^{-2}$, and Santos *et al.*⁴² obtained $\Delta z = 110$ Å at $T_s = 580$ °C and $N_s \approx 8 \times 10^{12} \text{ cm}^{-2}$. The width of silicon δ -layers was also determined directly: at $T_s = 550$ °C and an impurity density of 10^{13} cm^{-2} the experiments yielded 116 Å⁴³ and from 50 to 150 Å in different structures.⁴⁴ The main causes of the δ -layer broadening are diffusion due to the high growth temperature^{42,44} and segregation.⁴⁵

The electron density in the subbands as functions of the δ -layer thickness in the sample 2 are shown in Fig. 6. The best agreement with the Shubnikov–de Haas measurements is achieved at $\Delta z = 90$ Å in all the samples. The diagrams of the subbands calculated at this δ -layer width for the samples 2 and 6 are given in Fig. 7. One can see that the wave functions of the lower levels are localized in the δ -layer, and there are subbands with wave functions localized near the heterojunction. Higher subbands are common for both the heterojunction and δ -layer. The discrepancy between the calculated electron densities and Shubnikov–de Haas measurements are caused largely by the difference between the assumed δ -layer profile and its real shape (the impurity distribution may be not only inhomogeneous, but also asymmetrical with a tail in the growth direction⁴⁵), and by the effect of the contact layer on the Fermi-level position.

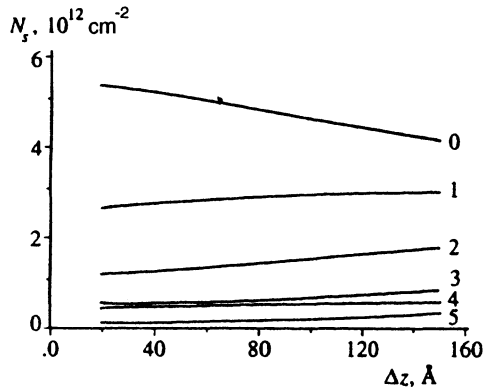


FIG. 6. Populations of subbands versus the width of the δ -layer for sample 2.

Calculation of the electron mobility due to scattering from ionized impurities when several subbands are filled

The transport mobility can be derived using the kinetic equation and describing the impurity scattering in the Born approximation.¹⁹ The scattering theory was generalized to the case of several filled subbands by Sigga and Kwok.⁴⁶ Below we describe the scheme for calculating transport relaxation times τ_n in the subbands (see also Refs. 25, 47–49).

When several dimensional subbands are filled, the τ_n are derived from the linear equation system

$$P_n(E)\tau_n(E) - \sum_{n \neq n'} P_{nn'}(E)\tau_{n'}(E) = 1, \quad (11)$$

where the coefficients $P_{nn'}$ are the probabilities for the respective intersubband transitions:

$$P_n(E) = \frac{m^*}{\pi \hbar^3} \int_0^\pi d\varphi (1 - \cos \varphi) |\tilde{V}_{nn}(q)|^2 + \frac{m^*}{\pi \hbar^3} \sum_{n \neq n'} \theta(E - E_{n'}) \int_0^\pi d\varphi |\tilde{V}_{nn'}(q')|^2, \quad (12)$$

$$P_{nn'}(E) = \frac{m^*}{\pi \hbar^3} \theta(E - E_{n'}) \left(\frac{E - E_{n'}}{E - E_n} \right)^{1/2} \times \int_0^\pi d\varphi \cos \varphi |\tilde{V}_{nn'}(q')|^2,$$

where

$$q = 2k(1 - \cos \varphi)^{1/2}, \quad q' = (k^2 - 2kk' \cos \varphi + k'^2)^{1/2},$$

$$k = [2m^*(E - E_n)/\hbar^2]^{1/2}, \quad k' = [2m^*(E - E_{n'})/\hbar^2]^{1/2},$$

and $\theta(x)$ is the Heavyside θ -function.

The effective scattering potential $\tilde{V}_{nn'}(q)$ takes into account the distribution of ionized impurities:

$$|\tilde{V}_{nn'}(q)|^2 = \int dz_i N(z_i) |\tilde{V}_{nn'}(q, z_i)|^2, \quad (13)$$

where $N(z_i)$ is the three-dimensional impurity density at the point z_i . Since the charged impurities are screened by free electrons of all the filled subbands, the matrix element of the nonscreened Coulomb potential,

$$V_{ll'}(q, z_i) = \frac{e^2}{2\varepsilon\varepsilon_0q} \int \psi_l(z) \exp(-q|z - z_i|) \psi_{l'}(z) dz, \quad (14)$$

is related to the screened potential $\tilde{V}_{nn'}(q, z_i)$ through the dielectric function:

$$\tilde{V}_{nn'}(q, z_i) = \sum_{ll'} \varepsilon_{nn', ll'}^{-1}(q) V_{ll'}(q, z_i), \quad (15)$$

where ε_0 is the permittivity of free space, ε is the dielectric constant, and $\psi_l(z)$ are the subband wave functions calculated concurrently with the band diagram. In the random-phase approximation the dielectric function has the form

$$\varepsilon_{ll', nn'}(q) = \delta_{ln} \delta_{l'n'} + \frac{e^2}{2\varepsilon\varepsilon_0q} F_{ll', nn'}(q) \Pi_{nn'}(q), \quad (16)$$

where $\Pi_{nn'}$ is the polarization component,⁴⁹ and the form-factor F is determined by the equation

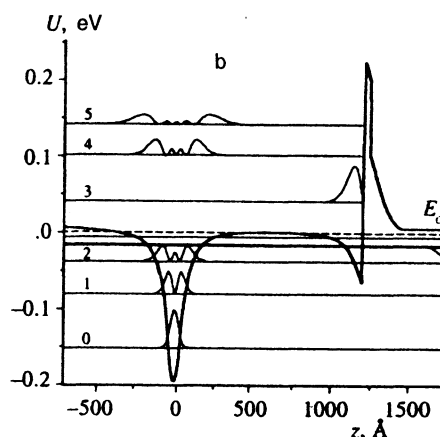
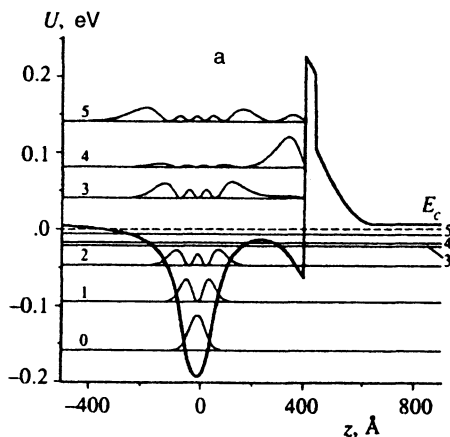


FIG. 7. Band diagrams of samples (a) 2 and (b) 6. The energy is measured with respect to the Fermi level (dashed line). Electron wave functions squared in subbands are also shown (those of the third, fourth, and fifth subband are shown at the tops of the graphs). E_c denotes the conduction-band bottom.

$$F_{ll',nn'}(q) = \int dz \int dz' \psi_l(z) \psi_{l'}(z) \times \exp(-q|z-z'|) \psi_n(z') \psi_{n'}(z'). \quad (17)$$

The transport mobility in the n th subband is

$$\mu_n = \frac{e}{m^*} \langle \tau_n(E) \rangle, \quad \langle \tau_n(E) \rangle = \frac{\int \tau_n(E) E \frac{\partial f_0(E)}{\partial E} dE}{\int E \frac{\partial f_0(E)}{\partial E} dE}, \quad (18)$$

where f_0 is the Fermi–Dirac distribution function. The quantum lifetime at the Fermi level is obtained by adding all the scattering probabilities with equal weights:⁴

$$\frac{1}{\tau_n^q} = \frac{m^*}{\pi \hbar^3} \sum_{n'} \int_0^\pi d\varphi |\tilde{V}_{nn'}(q')|^2, \quad \mu_n^q = \frac{e}{m^*} \tau_n^q. \quad (19)$$

The transport and quantum mobilities in samples 2, 3 and 6 calculated by this method are listed in Table I. The dependence of the mobility on the subband number is determined by several competing factors.¹⁰ On one hand, the Fermi momentum is lower in the higher subbands, which leads, according to the well-known properties of Coulomb scattering, to a lower mobility. On the other hand, the width of the electron localization region is larger in the higher subbands, i.e., the average separation between impurities and electrons is larger, which should result in a higher mobility. Therefore the shape of the function $\mu_n(n)$ cannot be easily derived from general considerations. Our numerical calculations (Table I) indicate that the electron mobility increases with the subband number. The mobility in the fourth subband (sample 3) or in the third subband (sample 6) is high because the δ -layer is at a considerable distance from the heterojunction, where the wave function of this subband is localized. In samples 3 and 6 the calculated transport mobility in the fourth and third subband, respectively ($> 10^5$ cm²/V·s), is one order of magnitude higher than that derived from mobility spectra (the mobility in the higher subbands could not be derived from Shubnikov–de Haas measurements because the electron densities in them were low and the corresponding Fourier components could not be detected in spectra of oscillations, see Fig. 5 and Table I), so alternative scattering mechanisms (mostly scattering due to the lateral roughness^{50,51}) should be taken into consideration. The calculations and measurements of mobilities are in good agreement, and the small discrepancies between the calculations and Shubnikov–de Haas measurements are, most probably, due to errors in the impurity distribution (which is important for the lower subbands) and in the calculated energy levels and wave functions (which affects mostly the mobility in higher subbands).

Optimization of transport parameters of heterostructures with combined doping

Figure 8 shows the conductivity σ and Hall mobility $\mu = R\sigma$ (the Hall coefficient R was measured at low magnetic fields) as functions of the distance L_δ between the

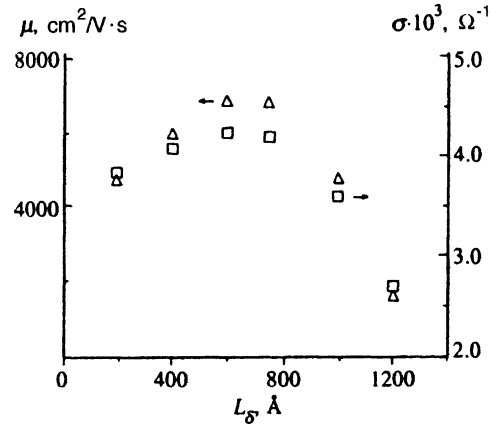


FIG. 8. Conductivity (squares) and Hall mobility (triangles) versus separation between the δ -layer and heterojunction at a temperature of 4.2 K in tested samples.

δ -layer and the heterojunction. Both the conductivity and Hall mobility have maxima at $L_\delta = 600\text{--}750$ Å.

The results described in the previous sections allow us to account for this dependence of the transport parameters on the distance L_δ . At small L_δ the electron scattering due to the impurities of the δ -layer is strong, so the mobilities in all the subbands are relatively low. The electron densities, as well as the mobility in the fourth subband, whose wave function is localized near the heterojunction increase with L_δ . Although this subband contributes only about one twentieth of the total electron density, it yields about one third of the conductivity owing to the high mobility. At larger distances between the junction and δ -layer the electron density in the higher subbands drops. As a result, there is an optimal distance between the heterojunction and δ -layer at which both the conductivity and Hall mobility are maximal.

It is noteworthy that the 2D-electron density in our samples was close to the limit for GaAs(Si). There are several publications demonstrating that the free-carrier density in δ -doped GaAs cannot be higher than 8×10^{12} cm⁻², although the dopant concentration may be considerably higher.^{16,39,43} In the sample 3 ($L_\delta = 600$ Å) the 2D-electron density is $N_s = 10.4 \times 10^{12}$ cm⁻², which is about 30% higher than the highest values reported for GaAs heterostructures. There are two interpretations of the electron density saturation in GaAs.^{18,52–54} The first (structural) mechanism is that at high silicon concentrations the dopant replaces not only Ga atoms to form donor centers, but also As, thus generating acceptors and compensating for the n -type conductivity. In this case the limiting electron density should depend on the growing conditions of a heterostructure. The second (electronic) mechanism is due to the impurity levels of the L -band, which is higher than the Γ -band in GaAs. The conduction band bends as the electron density increases, and when the Fermi level coincides with that of DX -centers (or similar centers with a sufficiently high density of states), the Fermi energy is pinned to the impurity level. In this case the free-electron density is determined by the energy difference between the Γ -band bottom and the DX -level, which equals about 200 meV in GaAs.^{39,52} The limiting electron density

measured as a function of pressure⁵³ provides evidence in favor of the electronic mechanism. The maximum energy differences between the Fermi level and Γ -band bottom measured in samples 2, 3, and 6 at 194, 198, and 196 meV, respectively, indicate that if the electronic saturation model is valid, the electron densities in these samples are close to maximum.

5. CONCLUSION

We have studied the electric transport properties of GaAs/Al_xGa_{1-x}As heterostructures in which Al_xGa_{1-x}As is uniformly doped with silicon and GaAs is δ -doped. The 2D-electron densities, transport and quantum mobilities in dimensional subbands have been derived from measurements of transverse magnetoresistance. The transport mobility in the upper subband is one order of magnitude higher than in the lower subbands, owing to the separation of free electrons from ionized impurities.

The electron densities, effective masses, and wave functions in all the subbands have been derived from self-consistent solutions of the Schrödinger and Poisson equations. The calculated electron mobilities due to scattering from ionized impurities in the case of several filled subbands are in good agreement with Shubnikov–de Haas measurements. Therefore the dependence of transport and quantum mobilities on the subband number in GaAs/AlGaAs heterostructures with combined doping at low temperatures can be ascribed to the impurity scattering. Intersubband carrier scattering affects mainly the mobility in the upper subbands: in the three lower subbands this scattering mechanism yields 20%, while in the upper subbands intrasubband carrier scattering and intersubband carrier scattering are comparable. The conductivity and Hall mobility have been measured as functions of the distance between the heterojunction and δ -layer. The Hall mobility and 2D-electron conductivity peak at a distance between the δ -layer and heterojunction $L_\delta = 600\text{--}750$ Å. This result is important for designing high-power transistors based on GaAs heterostructures with optimal parameters. The combination of the GaAs δ -doping and AlGaAs uniform doping has allowed us to manufacture heterostructures with the highest possible 2D-electron density of $1.04 \times 10^{13} \text{ cm}^{-2}$.

We are grateful to Prof. J. France and Dr. A. de Visser, who made it possible to carry out experiments in pulsed magnetic field at Amsterdam University (the Netherlands).

The work was supported by the International Science Foundation (Open Society Institute) and the Russian Fund for Fundamental Research (Grant No. 95-02-06021a).

¹H. van Houten, J. G. Williamson, M. E. I. Broekaart *et al.*, Phys. Rev. B **37**, 2756 (1988).

²R. Fletcher, E. Zaremba, M. D'Iorio *et al.*, Phys. Rev. B **38**, 7866 (1988).

³D. R. Leadley, R. J. Nicholas, J. J. Harris, and C. T. Foxon, Semicond. Sci. Technol. **5**, 1081 (1990).

⁴R. Fletcher, E. Zaremba, M. D'Iorio *et al.*, Phys. Rev. B **41**, 10649 (1990).

⁵P. T. Coleridge, Semicond. Sci. Technol. **5**, 961 (1990).

⁶Kyu-Seok Lee and El-Hang Lee, Phys. Rev. B **51**, 13315 (1995).

⁷S. Yamada and T. Makimoto, Appl. Phys. Lett. **57**, 1024 (1990).

⁸R. M. Kusters, F. A. Wittecamp, J. Singleton *et al.*, Phys. Rev. B **46**, 10207 (1992).

⁹J. P. Harrang, R. J. Higgins, R. K. Goodall *et al.*, Phys. Rev. B **32**, 8126 (1985).

¹⁰A. Ya. Shik, Fiz. Tverd. Tela **26**, 1161 (1992).

¹¹K. Ploog, M. Hauser, and A. Fischer, Appl. Phys. A **45**, 233 (1988).

¹²E. F. Shubert, J. E. Cunningham, W. T. Tsang, and G. L. Timp, Appl. Phys. Lett. **54**, 1350 (1989).

¹³L. R. Gonzalez, J. Krupski, and T. Szwacka, Phys. Rev. B **49**, 11111 (1994).

¹⁴E. F. Shubert, Loren Pfeiffer, K. W. West, and A. Izabelle, Appl. Phys. Lett. **54**, 1350 (1989).

¹⁵P. M. Koenraad, F. A. P. Blom, C. J. G. M. Langeraket *et al.*, Semicond. Sci. Technol. **5**, 861 (1990).

¹⁶A. Zrenner, F. Koch, and K. Ploog, Surf. Sci. **196**, 671 (1988).

¹⁷P. M. Koenraad, B. F. A. van Hest, F. A. P. Blom *et al.*, Physica B **177**, 485 (1992).

¹⁸E. Skuras, R. Kumar, R. L. Williams *et al.*, Semicond. Sci. Technol. **6**, 535 (1991).

¹⁹T. Ando, A. B. Fowler, and F. Stern, Rev. Mod. Phys. **54**, 437 (1982).

²⁰A. Isihara and L. Smrcka, J. Phys. C **19**, 6777 (1986).

²¹P. T. Coleridge, R. Stoner, and R. Fletcher, Phys. Rev. B **39**, 1120 (1989).

²²K. P. Martin, R. J. Higgins, J. J. L. Rascol *et al.*, Surf. Sci. **196**, 323 (1988).

²³F. F. Fang, T. P. Smith III, and S. L. Wright, Surf. Sci. **196**, 310 (1988).

²⁴S. Das Sarma and F. Stern, Phys. Rev. B **32**, 8442 (1985).

²⁵P. T. Coleridge, Phys. Rev. B **44**, 3793 (1991).

²⁶B. Das, S. Subramaniam, M. R. Melloch, and D. C. Miller, Phys. Rev. B **47**, 9650 (1993).

²⁷A. S. Rykov, *Searching for Optimum. Deformed Configuration Techniques* [in Russian], Nauka, Moscow (1993).

²⁸W. A. Beck and J. R. Anderson, J. Appl. Phys. **62**, 541 (1987).

²⁹I. A. Panaev, S. A. Studenikin, D. I. Lubyshev, and V. P. Migal, Semicond. Sci. Technol. **8**, 1822 (1993).

³⁰B. A. Al'tshuler, A. G. Aronov, A. N. Larkin, and D. E. Khmel'nitskiĭ, Zh. Éksp. Teor. Fiz. **81**, 768 (1981) [Sov. Phys. JETP **54**, 411 (1981)].

³¹H. J. Lee, L. Y. Juravel, J. C. Woolley, and A. J. Spring Thorpe, Phys. Rev. B **21**, 659 (1980).

³²M. Cheong Hyeonsik, J. H. Burnett, W. Paul *et al.*, Phys. Rev. B **49**, 10444 (1994).

³³H. Kroemer, Surf. Sci. **174**, 299 (1986).

³⁴N. March, W. Kohn, and P. Vashishta, *Theory of Nonuniform Electron Gas*, Mir, Moscow (1987).

³⁵F. Stern, S. Das Sarma, Phys. Rev. B **30**, 840 (1984).

³⁶B. Jonsson and S. T. Eng, IEEE J. Quant. Electr. **26**, 2025 (1990).

³⁷U. Ekenberg, Phys. Rev. B **40**, 7714 (1989).

³⁸Marcos H. Degani, Phys. Rev. B **44**, 5580 (1991).

³⁹S. P. Wilks, A. E. Cornish, M. Elliott *et al.*, J. Appl. Phys. **76**, 3583 (1994).

⁴⁰S. Fernandez de Avila, J. L. Sanchez-Rojas, F. Gonzalez-Sanz *et al.*, Appl. Phys. Lett. **64**, 907 (1994).

⁴¹F. Koch and A. Zrenner, Materials Science and Engineering **1**, 221 (1989).

⁴²M. Santos, T. Sajoto, A. Zrenner, and M. Shayegan, Appl. Phys. Lett. **53**, 2504 (1988).

⁴³J. J. Harris, Journal of Materials Science: Materials in Electronics **4**, 93 (1993).

⁴⁴E. F. Schubert, C. W. Tu, R. F. Kopf *et al.*, Appl. Phys. Lett. **54**, 2592 (1989).

⁴⁵J. C. Bezerra, A. G. de Oliveira, M. S. C. Mazzoni, and H. Chacham, J. Appl. Phys. **77**, 3283 (1995).

⁴⁶Eric D. Sigga and P. C. Kwok, Phys. Rev. B **2**, 1024 (1970).

⁴⁷S. Mori, T. Ando, J. Phys. Soc. Jap. **48**, 865 (1980).

⁴⁸G. Fishman and D. Calecki, Phys. Rev. B **29**, 5778 (1984).

⁴⁹K. Inoue and T. Matsuno, Phys. Rev. B **47**, 3771 (1993).

⁵⁰K. Hirakawa and H. Sakaki, Phys. Rev. B **33**, 8291 (1986).

⁵¹V. A. Kulbachinskiĭ, V. G. Kyin, V. I. Kadushkin *et al.*, J. Appl. Phys. **75**, 2081 (1994).

⁵²A. Zrenner, Appl. Phys. Lett. **55**, 156 (1989).

⁵³A. Zrenner, F. Koch, R. L. Williams *et al.*, Semicond. Sci. Technol. **3**, 1203 (1988).

⁵⁴J. J. Harris, R. Murray, and C. T. Foxon, Semicond. Sci. Technol. **8**, 31 (1993).

Translation was provided by the Russian Editorial office.